Multistate intermittency and extreme pulses in a fiber laser

A. N. Pisarchik*
Centro de Investigaciones en Optica, Loma del Bosque 115, 37150 Leon, Guanajuato, Mexico

R. Jaimes-Reátegui, R. Sevilla-Escoboza, and G. Huerta-Cuellar
Centro Universitario de los Lagos, Universidad de Guadalajara, Enrique Diaz de Leon 1144, Paseos de la Montaña, 47460 Lagos de Moreno, Jalisco, Mexico

(Received 8 June 2012; published 29 November 2012)

In our recent Letter [Phys. Rev. Lett. **107**, 274101 (2011)], we demonstrated that slow random perturbations of a system parameter were responsible for the emergence of rogue waves in a fiber laser with coexisting attractors. In this paper we investigate how the probability of a particular state to appear in multistate intermittency can be controlled by low-pass noise filtering. We show that the probability of some states depends nonmonotonously on the noise amplitude and cutoff frequency. The conditions for the emergence of extreme pulses in a erbium-doped fiber laser are analyzed numerically and experimentally.

DOI: 10.1103/PhysRevE.86.056219 PACS number(s): 05.45.−a, 05.40.Ca, 42.55.Wd, 42.60.Mi

I. INTRODUCTION

Because all natural systems have a stochastic component that affects their dynamics, many researchers in dissimilar areas of science have shown a great interest for the interaction between stochastic and deterministic processes. This is essentially appealing for multistable systems, where noise changes certain states stability, resulting in multistate intermittency. Such a behavior has been observed in many discrete and continuous systems.

The influence of noise on a system with coexisting attractors was first studied by Arecchi *et al.* [1], who observed noise-induced jumps between two coexisting states (two-state intermittency) in the forced Duffing oscillator with a double-well potential. Later a similar effect was found in multistable systems [2] and called *attractor hopping* [3] or *multistate intermittency* [4,5]. Relatively strong noise converts a multistable system into a metastable one, so that the phase-space trajectory, for a finite time, visits domains of different attracting sets.

In general, when discussing effects of noise on a multistable system, two distinct behaviors can be distinguished for weak noise and strong noise. While weak noise does not change the number of coexisting attractors and just modifies their basins of attraction, strong noise merges the basins in a new intermittent attractor, meaning that a trajectory visits intermittently distinct areas of phase space. Intermediate noise can induce bifurcations giving rise to multistability [6,7] and providing preference for some of attractors over the others [8–14]. These different noise effects have already been verified experimentally in a multistable erbium-doped fiber laser (EDFL) [4,5,15]. In particular, rare giant pulses referred to as *laser rogue waves* have been detected in the multistate intermittency regime when external white noise was cut off from the high-frequency side [5].

The study of rogue waves has increased drastically in recent years [16–18]. The giant pulses were found in both conservative and dissipative systems. Apart from the ocean [19], these waves have been discovered in the atmosphere [20], optics [21,22], plasmas [23], superfluids [24], Bose-Einstein condensates [25], capillars [26], and even finance [27]. The rogue waves in dissipative systems have been experimentally detected in semiconductor [28], Ti:sapphire [29], modulated fiber [5], Raman fiber [30], and mode-locked fiber [31] lasers. The laser rogue waves emerge as separate pulses of high intensity. One of the defining features of rogue waves in any system is an L-shape probability distribution function (PDF) of the wave amplitude, the same as ocean freak waves [32]. The manifestation of freak waves in different systems is of great scientific interest; debates about their common features and differences still continue [33]. Further research on rogue waves in any field of science and in nature enriches their concept leading towards a deeper understanding of this interesting phenomenon which is not yet widely explored.

In this work, we study noise-induced multistate intermittency in the EDFL with coexisting attractors. The EDFL is a very practical dynamical system for studying multistability and its control [4,5,13,15,34–38] because the coexisting attractors can be easily distinguished by their pulse frequencies and amplitudes, which make the laser rogue waves measurement less demanding. It is widely accepted by many researchers that the amplitude of the extreme pulses should be at least double of the most probable pulse amplitude. We will analyze conditions for the emergence of rogue waves in the EDFL and show how the probability of the appearance of extreme pulses can be controlled by noise parameters, in particular, noise amplitude and cutting frequency of a low-pass filter.

The paper is organized as follows. In Sec. II we start with model equations, and then we present results of numerical simulations. Section III is devoted to the experimental study of EDFL dynamics under periodic and stochastic modulation. First, we describe our experimental setup and then we present experimental results and compare them with the numerical ones. Finally, main conclusions are given in Sec. IV.

*apisarch@cio.mx

II. NUMERICAL SIMULATIONS

A. Model

The dynamics of the diode-pumped EDFL is described by the following equations [5,38]:

$$\frac{dP}{dt} = \frac{2L}{T_r} P\{r_w \alpha_0 [N(\xi_1 - \xi_2) - 1] - \alpha_{\text{th}}\} + P_{\text{sp}}, \quad (1)$$

$$\frac{dN}{dt} = -\frac{\sigma_{12} r_w P}{\pi r_0^2}(N\xi_1 - 1) - \frac{N}{\tau} + P_{\text{pump}}, \quad (2)$$

where P is the intracavity laser power, $N = (1/n_0 L)\int_0^L N_2(z)\,dz$ is the averaged (over the active fiber length L) population of the upper lasing level, N_2 is the upper level population at the z coordinate, n_0 is the refractive index of a "cold" erbium-doped fiber core, ξ_1 and ξ_2 are parameters defined by the relationship between cross sections of ground state absorption (σ_{12}), return stimulated transition (σ_{12}), and exited state absorption (σ_{23}). T_r is the photon intracavity round-trip time, α_0 is the small-signal absorption of the erbium fiber at the laser wavelength, α_{th} accounts for the intracavity losses on the threshold, τ is the lifetime of erbium ions in the excited state, r_0 is the fiber core radius, w_0 is the radius of the fundamental fiber mode, and r_w is the factor addressing a match between the laser fundamental mode and erbium-doped core volumes inside the active fiber. The spontaneous emission into the fundamental laser mode is derived as

$$P_{\text{sp}} = N\frac{10^{-3}}{\tau T_r}\left(\frac{\lambda_g}{w_0}\right)^2 \frac{r_0^2 \alpha_0 L}{4\pi^2 \sigma_{12}}, \quad (3)$$

where λ_g is the laser wavelength. The pump power is expressed as

$$P_{\text{pump}} = P_p \frac{1 - \exp[-\alpha_0 \beta L(1 - N)]}{N_0 \pi r_0^2 L}, \quad (4)$$

where P_p is the pump power at the fiber entrance and β is a dimensionless coefficient. We explore the following parameter values: $L = 0.88$ m, $T_r = 8.7$ ns, $r_w = 0.308$, $\alpha_0 = 40$ m^{-1}, $\xi_1 = 2$, $\xi_2 = 0.4$, $\alpha_{th} = 3.92 \times 10^{-2}$, $\sigma_{12} = 2.3 \times 10^{-17}$ m^2, $r_0 = 2.7 \times 10^{-6}$ m, $\tau = 10^{-2}$ s, $\lambda_g = 1.65 \times 10^{-6}$ m, $w_0 = 3.5 \times 10^{-6}$ m, $\beta = 0.5$, and $N_0 = 5.4 \times 10^{25}$ m^{-3}. These parameters correspond to the real experimental conditions described in Sec. III. Although the model was designed for a single-mode laser, it describes well the dynamics of a longitudinally multimode erbium-doped fiber laser if only power characteristics are exploited.

B. Coexisting attractors

Under harmonic modulation

$$P_p = p[1 - m\sin(2\pi f_d t)] \quad (5)$$

applied to the diode pump current, the EDFL described by Eqs. (1) and (2) exhibits the coexistence of up to four attractors: period 1 (P1), period 3 (P3), period 4 (P4), and period 5 (P5). In Eq. (5), p is the pump power without modulation, i.e., when $m = 0$. The branches of the coexisting attractors are clearly seen in the bifurcation diagrams of the laser peak power shown in Fig. 1. These diagrams are obtained by varying initial conditions and using the modulation frequency f_d and amplitude m as control parameters. The stable periodic

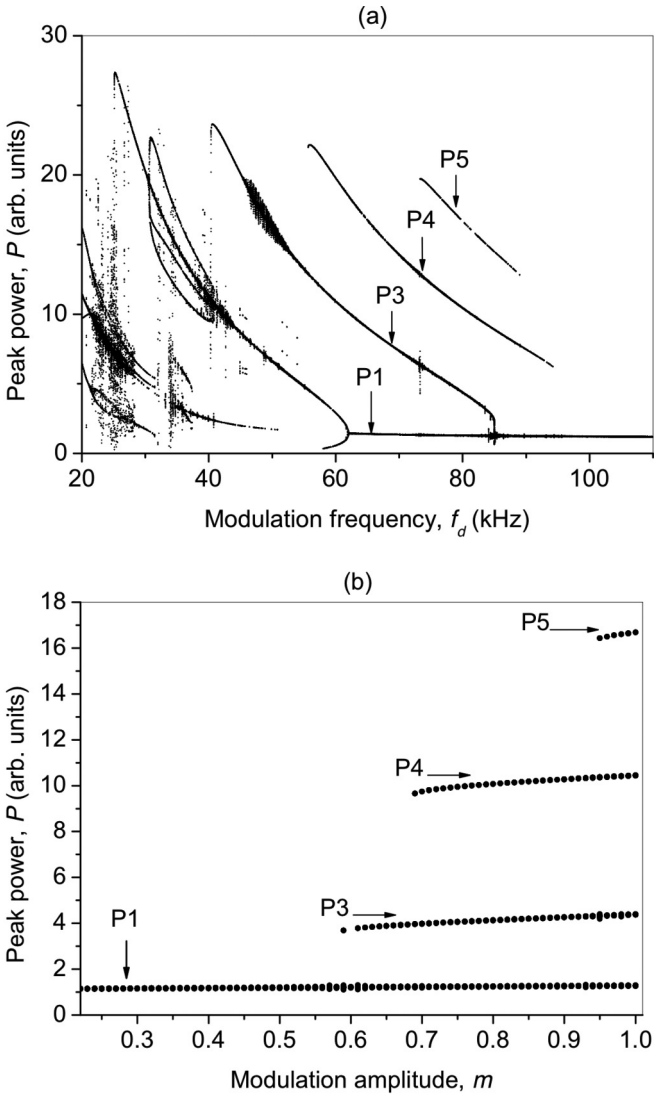

FIG. 1. Numerical bifurcation diagrams of laser peak power as functions of (a) driving frequency f_d for $m = 1$ and (b) driving amplitude m for $f_d = 80$ kHz. The diagrams are calculated by varying initial conditions and using the continuation method. The branches of the coexisting periodic orbits P1, P3, P4, and P5 are shown by the arrows.

orbits on subharmonic frequencies (P3, P4, and P5) are born in saddle-node bifurcations when the control parameter is increased.

Figure 2 shows the basins of attraction of the coexisting stable periodic orbits for fixed $f_d = 80$ kHz and different m. While for low modulation amplitudes, the laser is monostable with a single P1 [Fig. 2(a)], the subharmonic attractors of P3 [Fig. 2(b)] and P4 [Fig. 2(c)] emerge, and the sizes of their basins of attraction enlarge when m is increased, while the P1 basin's volume decreases, as shown in Fig. 3.

C. Stochastic modulation

When both harmonic and random signals are added to the pump current as

$$P_p = p[1 - m_d \sin(2\pi f_d t) + \eta G(\zeta, f_n)], \quad (6)$$

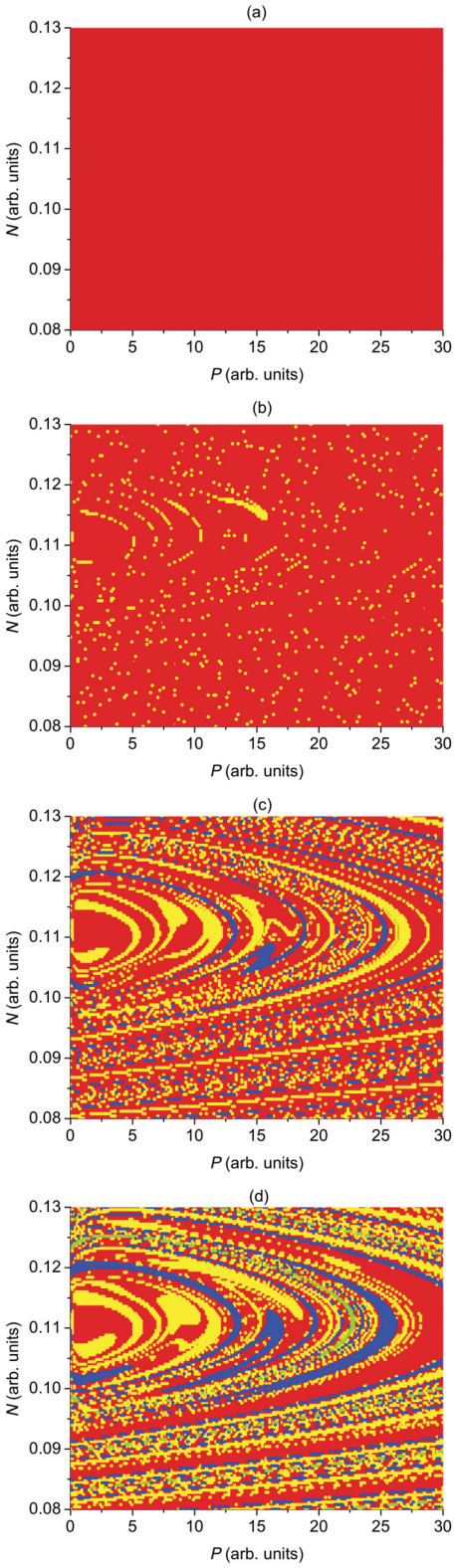

FIG. 2. (Color online) Basins of attraction of four coexisting attractors in EDFL under pump modulation with $f_d = 80$ kHz and (a) $m = 0.4$, (b) $m = 0.6$, (c) $m = 0.8$, and (d) $m = 1$. P1, P3, and P4 are shown, respectively, by the red (gray), yellow (light gray), and blue (dark gray) dots.

intermittent switches between different coexisting periodic regimes occur. Here η is the noise amplitude and $G(\zeta, f_n)$

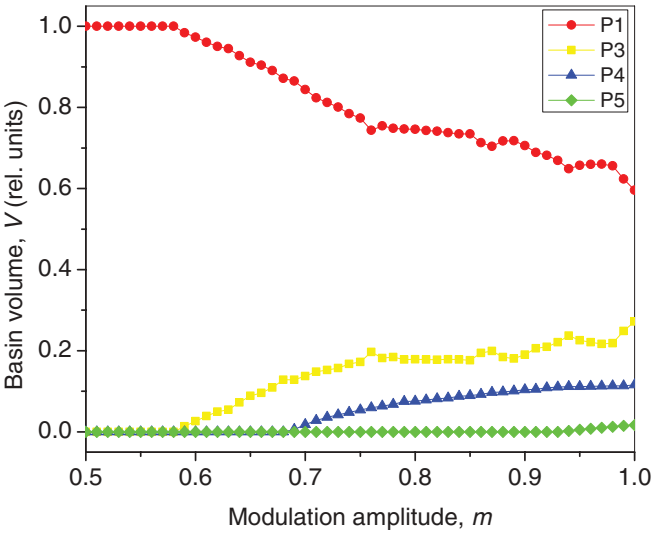

FIG. 3. (Color online) Relative volumes of basins of attraction of coexisting attractors in EDFL as a function of modulation amplitude for $f_d = 80$ kHz.

is the zero-mean noise function in terms of a random number $\zeta \in [-1, 1]$ and the noise low-pass cutoff frequency f_n (white noise is filtered with a fifth order discrete low-pass Butterworth filter in LabVIEW 8.5). The application of Gaussian white noise with the first order filter does not result in a significant difference [39].

The parameters of stochastic modulation, f_n and η, are varied to change the number of coexisting attractors and the preference of different periodic regimes which appear in multistate intermittency. Figure 4 shows the location of different intermittency states in the space of the noise parameters. This diagram is calculated for the fixed initial conditions corresponding to P1. For small-amplitude noise, P1 is always stable, and it coexists with other attractors (P3 and P4) for any f_n. For stronger noise, the laser works in the intermittent regimes; depending on the noise parameters, the laser switches either between P1 and P3, or between P1, P3, and P4, or between P1, P3, P4, and P5. Note, that the P5 oscillations appear only in the intermittent regime; i.e., for the explored parameters the P5 is unstable, even in the absence of noise.

It is particularly remarkable that the large-amplitude subharmonic oscillations appear in the intermittent regimes only when noise contains just low frequency components, i.e., P4 is observed only for $f_n < 1$ MHz [Fig. 4(a)] and P5 for $f_n < 200$ kHz [Fig. 4(b)]. As seen from Fig. 4(b), the minima of the boundaries between the intermittency regions occur at the fundamental (relaxation oscillation) laser frequency $f_r \approx 30$ kHz. This means that when noise is cut off at this frequency, it is much easier to obtain subharmonic oscillations. Indeed, as seen in Fig. 5, the probability for the appearance of the subharmonic pulses increases as f_n is decreased, while the probability of P1 goes down. Since the amplitudes of the P4 and P5 pulses are much larger than the amplitude of the P1 pulses, they can be treated as extreme pulses, but only when their appearance probability is very low [5]. Therefore, the extreme pulses (P4 or P5) can emerge only in a certain small region of

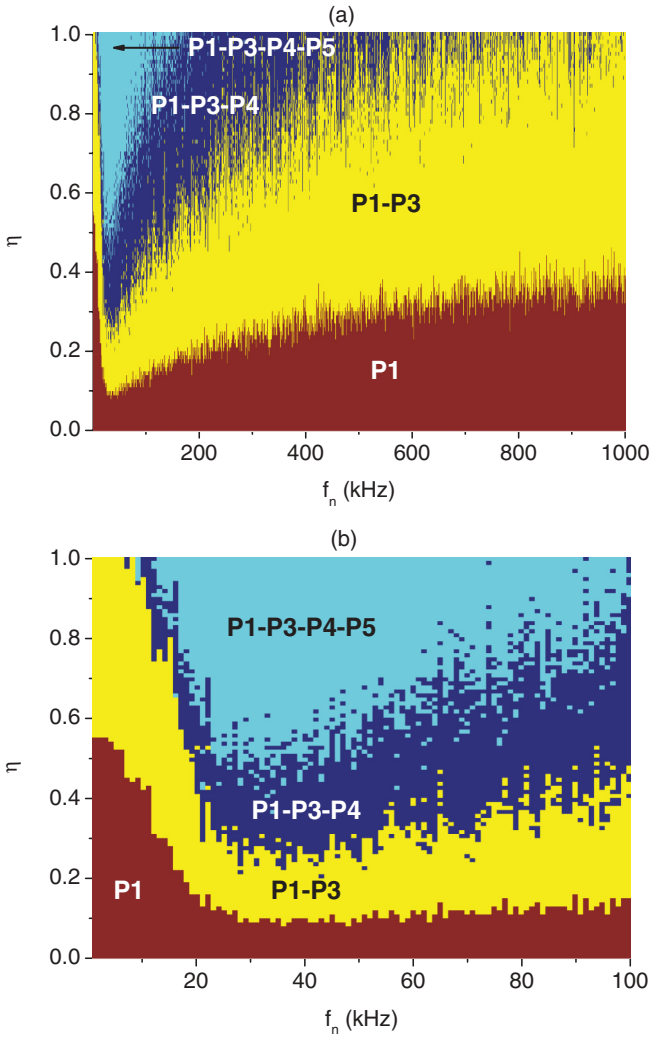

FIG. 4. (Color online) Numerical state diagram in space of noise parameters in (a) wide frequency range and (b) enlarged low frequency range. Three attractors coexist in the brown (black) region (P1, P3, and P4). Intermittency between two states (P1 and P3) is observed in the yellow (gray) region, between three states (P1, P3, and P4) in the blue (dark gray), and between four states (P1, P3, P4, and P5) in the magenta (light gray) region. $m = 1$ and $f_d = 80$ kHz.

noise parameters. The probability distributions obtained with Gaussian white noise are very similar [39].

Figure 6 shows the probability as a function of the noise amplitude for three fixed cutoff frequencies (5, 30, and 90 kHz). While P1 appears with 100% probability for small noise ($\eta < 0.2$) [Fig. 6(a)], the probability diminishes as the noise amplitude is increased, giving rise to other regimes. The interesting feature of these dependencies is that the probability of some states depends nonmonotonously on the noise amplitude. In particular, the probability of P3 has a maximum $W^{\max}$ for a certain noise amplitude $\eta^{\max}$ [Fig. 6(b)]; i.e., there exists a certain noise level for which the P3 regime is more likely to occur than for any other noise amplitude. A similar nonmonotonous dependence has been recently found in preference of some attractors in the multistable Hénon map subject to stochastic modulation [14]. Although more detailed study of this phenomenon is required, our preliminary

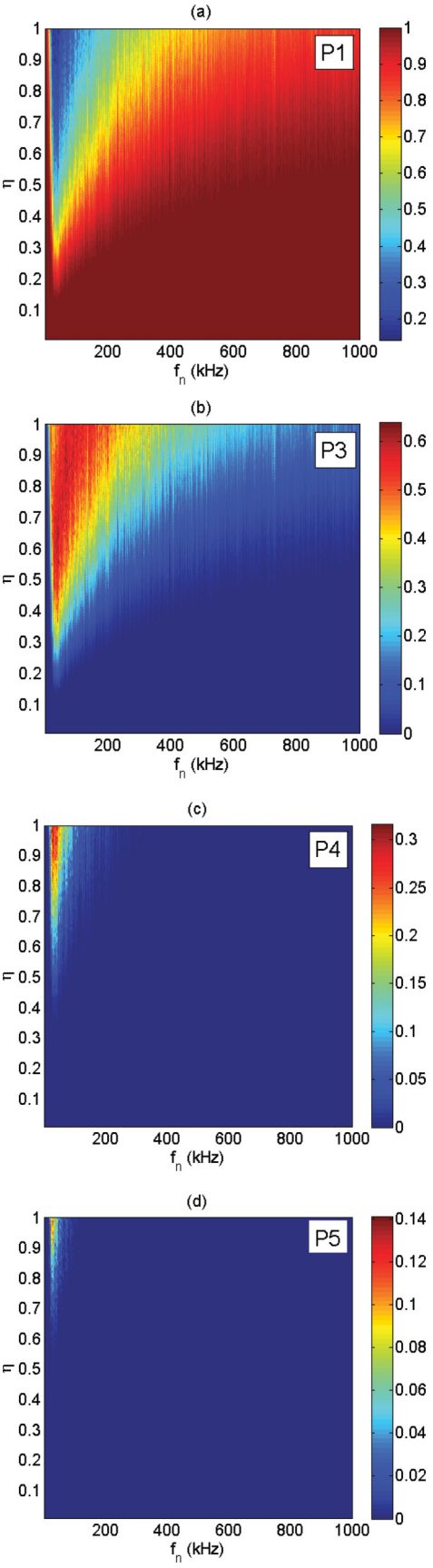

FIG. 5. (Color online) Probability densities for (a) P1, (b) P3, (c) P4, and (d) P5 regimes in (f_n, η) parameter space. $m = 1$ and $f_d = 80$ kHz.

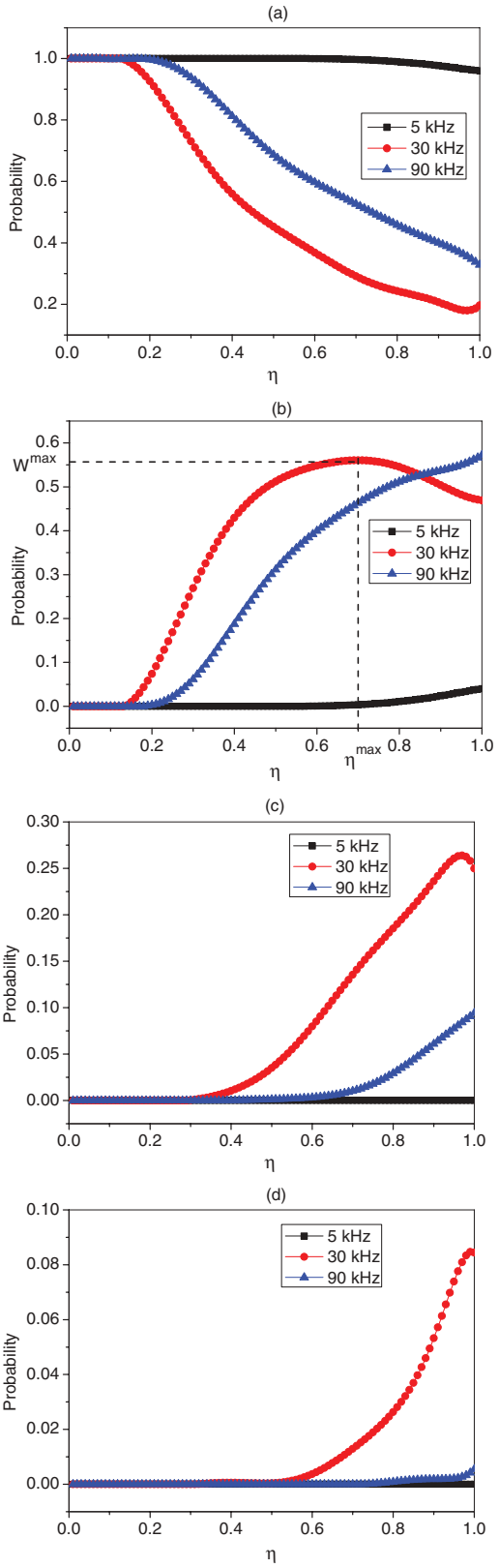

FIG. 6. (Color online) Probability of (a) P1, (b) P3, (c) P4, and (d) P5 oscillations versus noise amplitude η for three fixed cutting frequencies f_n of low-pass noise filter. The position of the maximum ($\eta^{\max}$ and $W^{\max}$) in the noise-dependent probability of P3 is shown by the dashed lines in (b).

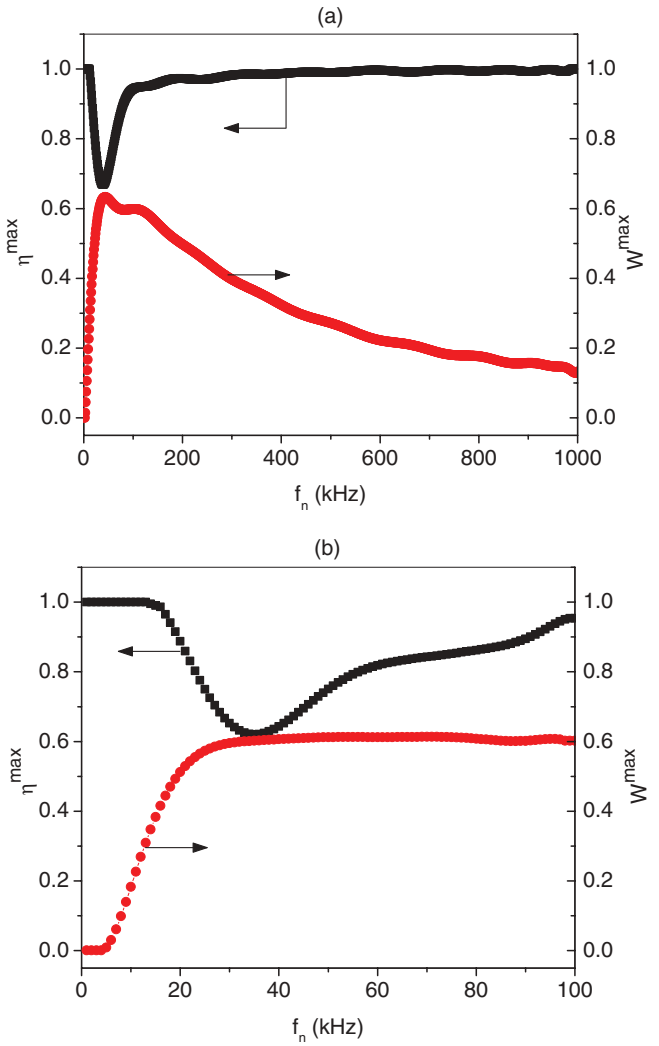

FIG. 7. (Color online) Position of noise-dependent probability maximum for P3 as a function of noise cutoff frequency f_n in (a) wide frequency range and (b) enlarged low frequency range.

results allow us to hypothesize that such behavior originates from stochastic resonance resulting from the interaction of the driving frequency with the Kramers time of a particular state.

The position of the probability maximum depends on f_n. Both the maximum probability $W^{\max}$ of P3 and the corresponding noise amplitude $\eta^{\max}$ are plotted in Fig. 7 as functions of f_n. One can see that the absolute probability maximum occurs when f_n is close to f_r at the minimum noise amplitude.

III. EXPERIMENT

A. Experimental setup

The experimental setup shown in Fig. 8 consists of a 1560-nm EDFL pumped by a 977-nm laser diode (LD) (PL980). The 4.81-m Fabry-Perot fiber laser cavity is formed by an active 88-cm-long heavily erbium-doped fiber (EDF) with a 2.7-μm core diameter and two fiber Bragg gratings (FBG1 and FBG2) with 0.288-nm and 0.544-nm full widths on half-magnitude bandwidth, having, respectively, 100% and

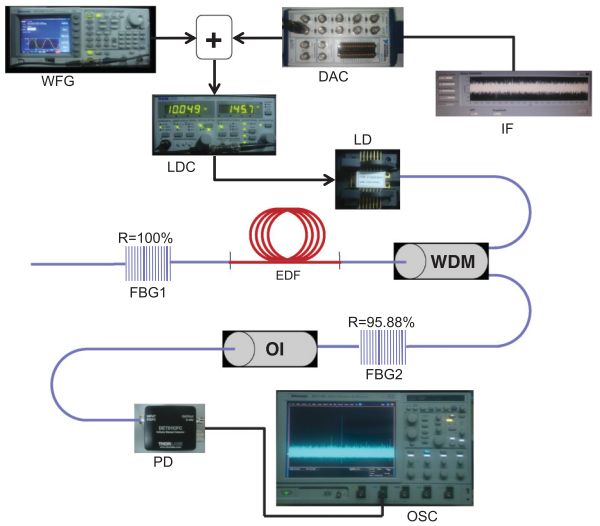

FIG. 8. (Color online) Experimental setup. A fiber laser formed by an erbium-doped fiber (EDF) and two fiber Bragg gratings (FBG1 and FBG2) is externally driven by both harmonic and noisy signals applied to a diode pump laser (LD) current via a laser diode controller (LDC) from a wave function generator (WFG) and a noise interface (IF) through a digital-to-analogical converter (DAC). The fiber laser output after passing through a wavelength-division multiplexer (WDM) and an optical isolator (OI) is recorded with a photodiode (PD) and analyzed with a digital oscilloscope (OSC).

95.88% reflectivities at the laser wavelength. All optical components are connected by a single-mode fiber. The diode pump laser is controlled by a laser diode controller (LDC) (Thorlabs ITC510). In our experiments, the diode current is fixed at 145.5 mA, which corresponds to a 20-mW pump power, while the EDFL threshold occurs at 110 mA. This pump current is chosen to ensure the laser relaxation oscillation frequency around $f_r = 30$ kHz. To drive the EDFL, the sum of harmonic and random signals, $m\sin(2\pi f_d t) + \eta G(\zeta, f_n)$, is applied to the diode pump current from a wave function generator (WFG) (Tektronix AFG3102) and a noise interface (IF), respectively. The periodic and random signals are summed at the input of the current controller of the diode laser through corresponding independent resistors providing a 500-kHz bandwidth of the summation circuit.

In our experiments, we explore the same noise as in the numerical simulations; i.e., the noise is generated by LabVIEW 8.5 and then converted to the analog signal using a digital-to-analog converter (DAC) (Tektronix AFG3102) with the 5MS/s sampling rate. Noise with $\eta = 1$ V results in a 50% modulation depth of the pump current; both the average pump current and f_r are independent of the noise amplitude. The influence of noise on the relaxation oscillation frequency has been extensively studied in Ref. [15].

B. Bifurcation and state diagrams

Using f_d and m as control parameters, we construct the experimental bifurcation diagrams of the laser peak intensity shown in Fig. 9. The diagrams are obtained using times series for different values of the control parameters. The experimental dynamics confirms the results of numerical

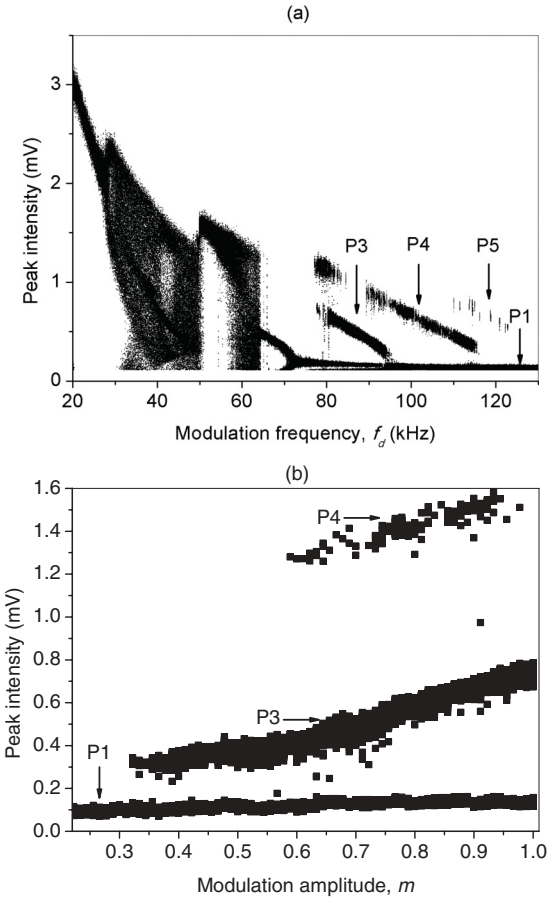

FIG. 9. Experimental bifurcation diagrams of laser peak intensity versus (a) driving frequency f_d for $m = 0.8$ and (b) driving amplitude m for $f_d = 90$ kHz. The diagrams are calculated by switching on and off the signal generator. The arrows point to the branches of the coexisting periodic orbits P1, P3, P4, and P5.

simulations, providing a qualitative similarity (compare with Fig. 1). Although the relaxation oscillation frequencies in the experiment and numerical simulations coincide ($f_r = 30$ kHz), there is a small difference for higher driving frequencies, where the experimental bifurcation diagrams are shifted by 10 kHz. We hypothesize that this shift may be caused by internal noise inherent to semiconductor and fiber lasers, which was not included in the model. The experimental noise is also responsible for the broadening of the attractor branches in the bifurcation diagrams in Fig. 9.

As in the simulations, we explore the parameter range where EDFL exhibits coexistence of attractors. In particular, we fix the modulation parameters at $f_d = 90$ kHz and $m = 0.8$ V, for which P1, P3, and P4 coexist, and apply additional random modulation to the laser diode pump current.

The experimental state diagram in the (f_n, η) parameter space is presented in Fig. 10. Similarly to the numerical one in Fig. 4, it confirms that P1 is stable only for small-amplitude noise. When η is increased, P1 loses its stability, and the laser switches among other coexisting periodic regimes resulting in multistate intermittency [4]. Although in general the numerical and experimental diagrams look similar, a small difference appears for low f_n. This difference can be explained by the following reasons: first, in the simulations the initial conditions

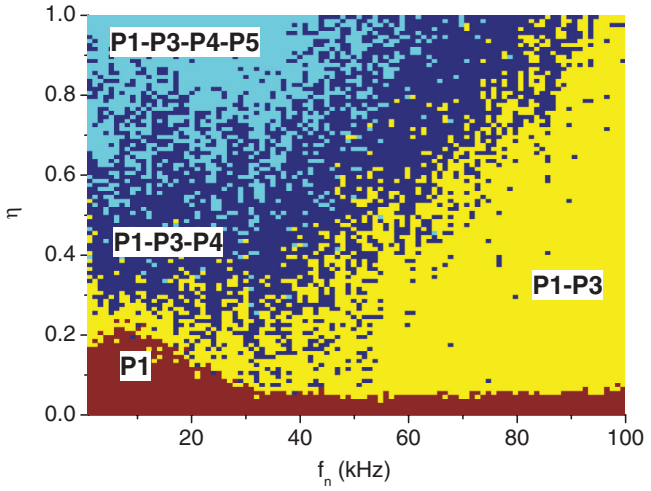

FIG. 10. (Color online) Experimental state diagram in the (f_n,η) noise parameters space. The subharmonic regimes P4 and P5 with large-amplitude pulses appear in multistate intermittency when noise is filtered for low frequencies. $f_d = 90$ kHz and $m = 0.8$ V.

are fixed for P1, while in the experiment they are random since the experimental control of initial conditions is next to impossible; and second, there exist uncontrolled proper white and $1/f$ noises inherent to semiconductor and fiber lasers [40,41], which may result in intermittency for smaller level of external noise.

C. Multistate intermittency and rogue waves

Figure 11(a) shows the oscilloscope traces recorded at fixed $f_n = 30$ kHz and various η, and the corresponding PDFs of the pulse intensities are displayed in Fig. 11(b). The extreme pulses of P4 are depicted for $\eta = 0.25$ V because in this specific regime the PDF approximates an L shape. We should underline that the extreme pulses usually appear at the borders between the intermittent regimes in Fig. 10, where the probability of such events is very low. Due to internal laser noise, the rogue waves in the experiment emerge for lower amplitude of external noise than in the simulations.

The variation of the noise amplitude and cutoff frequency, f_n and η, allows us to control the probability for different coexisting states. Figure 12 shows the experimental probabilities of the appearance of P1 [Fig. 12(a)], P3 [Fig. 12(b)], P4 [Fig. 12(c)], and P5 [Fig. 12(d)]. The rogue waves of P4 and P5 can be seen as separated light dots in Figs. 12(c) and 12(d).

Last, the noise dependencies of the probability of every periodic state in the intermittency regime are shown in Fig. 13 for three different f_n. The experiment confirms the nonmonotonous character of these dependencies for some coexisting states, which was predicted numerically in Sec. II. This is clearly seen in Fig. 13(b), where the probability of P3 for $f_n = 5$,30, and 90 kHz has maxima at $\eta \approx 0.7$, 0.35, and 0.95, respectively. The position of these maxima as a function of f_n is shown in Fig. 14. The maximum of $W^{\max}$ occurs close to $f_r = 30$ kHz that corresponds to the minimum $\eta^{\max}$; this also confirms the results of the numerical simulations. A small discrepancy between the numerical and experimental dependencies in Fig. 7(b) and Fig. 14 in the

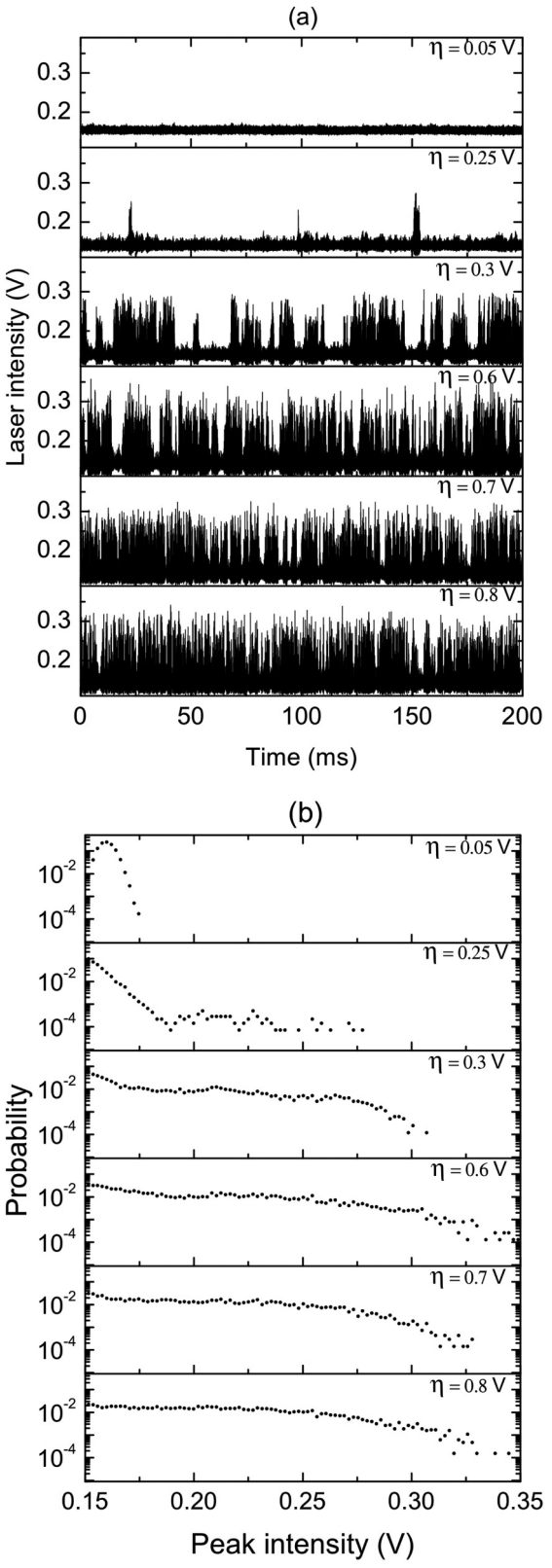

FIG. 11. (a) Experimental time series of laser intensity and (b) corresponding probability distributions of peak intensities for different noise amplitudes. $f_n = 30$ kHz, $f_d = 90$ kHz, and $m = 0.8$ V. The extreme pulses for $\eta = 0.25$ V exhibit a nearly L-shape PDF.

low-frequency range can be again explained by the presence of $1/f$ quantum noise. Low-frequency components of the

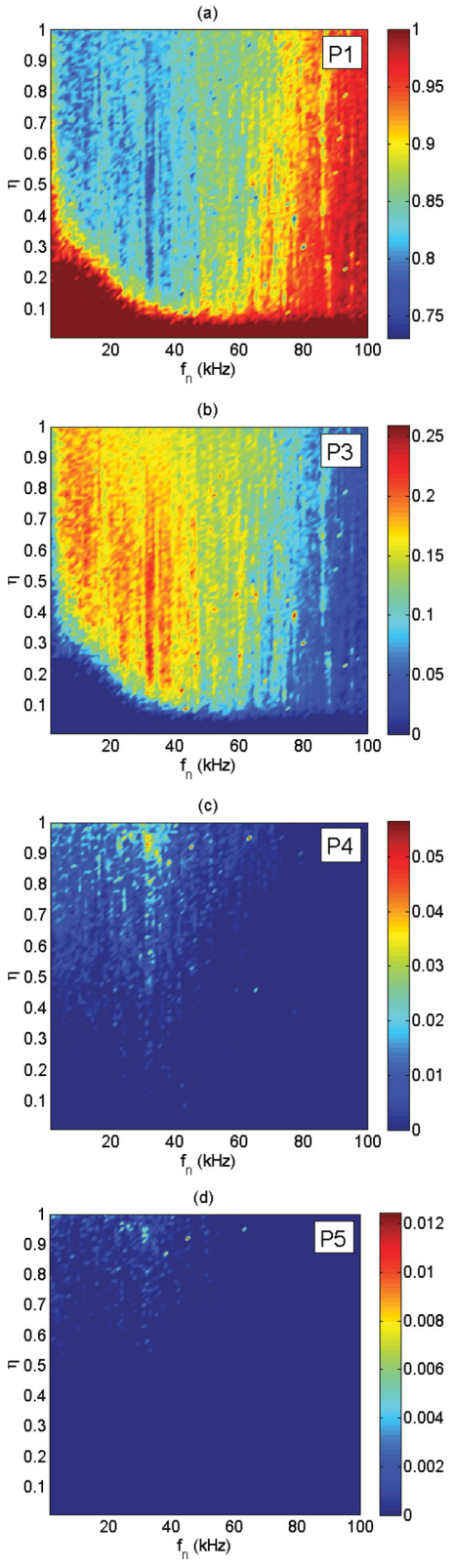

FIG. 12. (Color online) Experimental probabilities of different intermittent states in (f_n, η) parameter space for (a) P1, (b) P3, (c) P4, and (d) P5. $f_d = 90$ kHz and $m_d = 0.8$ V.

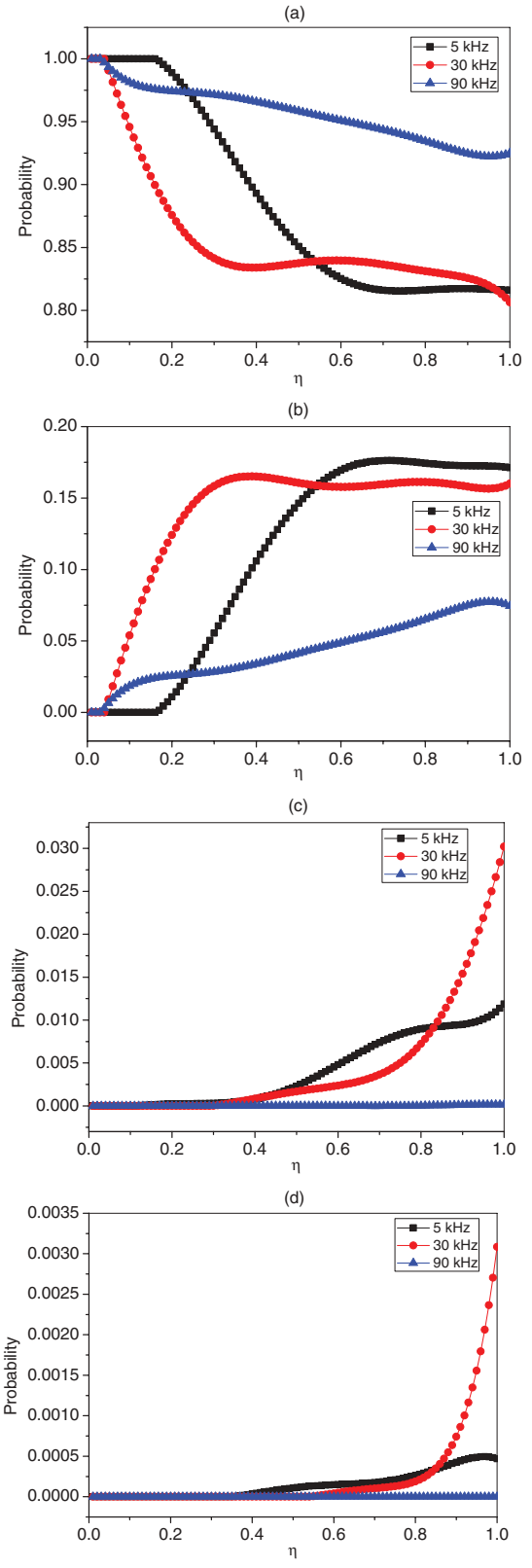

FIG. 13. (Color online) Experimental probabilities of different intermittent states as functions of noise amplitude for three different f_n for (a) P1, (b) P3, (c) P4, and (d) P5.

internal laser noise destabilizes the P1 attractor, thus leading to increasing probability for the appearance of subharmonic oscillations.

The above statistical analysis demonstrates good agreement between experimental and numerical results, indicating that

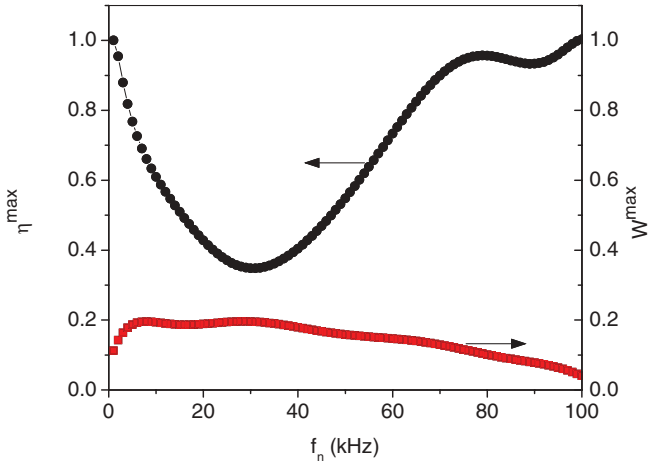

FIG. 14. (Color online) Experimental position of maximum noise-dependent probability for P3 as a function of noise cutoff frequency f_n.

the model captures the fundamental aspects of our experimental system.

IV. CONCLUSION

In this work, we have demonstrated how multistate intermittency in EDFL can be controlled by adjusting noise parameters, i.e., by varying the noise amplitude η and the low-pass filter frequency f_n. The interaction of harmonic and stochastic modulation with the laser relaxation oscillation frequency f_r induces preference for some states in a multistate intermittency regime, which depends on the noise parameters η and f_n. While the maximum probability of subharmonic oscillations occurs when f_n is close to f_r, laser rogue waves are detected for $f_n < f_r$, where the appearance of the subharmonic states is less probable.

Our model demonstrates a fundamental understanding of the system dynamics and gives insight into the nontrivial effects arising in the experiment, such as extreme pulses and noise-induced preference of some states. Due to uncontrolled internal laser noise, the extreme pulses in the experiment appear for smaller amplitudes of external noise than in the numerical simulations.

Finally, we have also shown that the preference of some states in multistate intermittency depends nonmonotonously on the noise amplitude; i.e., there exists a certain noise level for which a particular state is more probable than for other noise amplitudes. This result is in agreement with previously reported nonmonotonous attractor preference observed in the multistable Hénon map [14]. The resonance character of the noise dependence may be of interest for potential applications in communication with multistable systems exploiting stochastic resonances between different coexisting states, which can be a topic for future research.

ACKNOWLEDGMENT

The authors acknowledge CONACYT (Mexico) for the financial support through Project No. 100429.

[1] F. T. Arecchi, R. Badii, and A. Politi, Phys. Rev. A **32**, 402 (1985).
[2] K. Wiesenfeld and P. Hadley, Phys. Rev. Lett. **62**, 1335 (1989).
[3] S. Kraut and U. Feudel, Phys. Rev. E **66**, 015207(R) (2002).
[4] G. Huerta-Cuellar, A. N. Pisarchik, and Y. O. Barmenkov, Phys. Rev. E **78**, 035202(R) (2008).
[5] A. N. Pisarchik, R. Jaimes-Reátegui, R. Sevilla-Escoboza, G. Huerta-Cuellar, and M. Taki, Phys. Rev. Lett. **107**, 274101 (2011).
[6] A. E. Barbéroshie, I. I. Gontsya, Y. N. Nika, and A. K. Rotaru, J. Exp. Theor. Phys. **77**, 211 (1993).
[7] S. Kim, S. H. Park, and C. S. Ryu, Phys. Rev. Lett. **78**, 1616 (1997).
[8] S. Kraut, U. Feudel, and C. Grebogi, Phys. Rev. E **59**, 5253 (1999).
[9] K. Kaneko, Phys. Rev. Lett. **78**, 2736 (1997).
[10] K. Kaneko, Physica D **124**, 322 (1998).
[11] A. N. Pisarchik, in *Some Topics of Modern Optics*, edited by R. Rodriguez-Vera and F. Mendoza-Santoyo (Rinton Press, Kerala, 2008), pp. 326–391.
[12] B. K. Goswami and A. N. Pisarchik, Int. J. Bifurcat. Chaos **18**, 1645 (2008).
[13] A. N. Pisarchik and R. Jaimes-Reátegui, Phys. Lett. A **374**, 228 (2009).
[14] B. E. Martínez-Zérega and A. N. Pisarchik, Commun. Nonlin. Sci. Numer. Simulat. **17**, 4023 (2012).
[15] G. Huerta-Cuellar, A. N. Pisarchik, A. V. Kir'yanov, Yu. O. Barmenkov, and J. del Valle Hernandez, Phys. Rev. E **79**, 036204 (2009).
[16] K. Dysthe, H. E. Krogstad, and P. Muller, Annu. Rev. Fluid Mech. **40**, 287 (2008).
[17] E. Pelinovsky and C. Kharif, *Extreme Ocean Waves* (Springer, Berlin, 2008).
[18] A. R. Osborne, *Nonlinear Ocean Waves and the Inverse Scattering Transform* (Elsevier, London, 2010).
[19] C. Garrett and J. Gemmrich, Phys. Today **62**, 57 (2009).
[20] L. Stenflo and P. K. Shukla, J. Plasma Phys. **75**, 841 (2009).
[21] D. R. Solli, C. Ropers, P. Koonath, and B. Jalali, Nature (London) **450**, 1054 (2007).
[22] M. Erkintalo, G. Genty, and J. M. Dudley, Opt. Lett. **34**, 2468 (2009).
[23] W. M. Moslem, P. K. Shukla, and B. Eliasson, Europhys. Lett. **96**, 25002 (2011).
[24] V. B. Efimov, A. N. Ganshin, G. V. Kolmakov, and P. V. E. McClintock, Eur. Phys. J. Special Topics **185**, 181 (2011).
[25] Y. V. Bludov, V. V. Konotop, and N. Akhmediev, Phys. Rev. A **80**, 033610 (2009).
[26] M. Shats, H. Punzmann, and H. Xia, Phys. Rev. Lett. **104**, 104503 (2010).
[27] Z.-Y. Yan, Commun. Theor. Phys. **54**, 947 (2010).
[28] C. Bonatto, M. Feyereisen, S. Barland, M. Giudici, C. Masoller, J. R. Rios Leite, and J. R. Tredicce, Phys. Rev. Lett. **107**, 053901 (2011).

[29] M. G. Kovalsky, A. A. Hnilo, and J. Tredicce, Opt. Lett. **36**, 4449 (2011).
[30] S. Randoux and P. Suret, Opt. Lett. **37**, 500 (2012).
[31] C. Lecaplain, Ph. Grelu, J. M. Soto-Crespo, and N. Akhmediev, Phys. Rev. Lett. **108**, 233901 (2012).
[32] C. Kharif, E. Pelinovsky, and A. Slunyaev, *Rogue Waves in the Ocean* (Springer-Verlag, Heidelberg, 2009).
[33] N. Akhmediev and E. Pelinovsky, Eur. Phys. J. Special Topics **185**, 1 (2010).
[34] J. M. Saucedo-Solorio, A. N. Pisarchik, A. V. Kir'yanov, and V. Aboites, J. Opt. Soc. Am. B **20**, 490 (2003).
[35] A. N. Pisarchik, Yu. O. Barmenkov, and A. V. Kiryanov, IEEE J. Quantum Electron. **39**, 1567 (2003).
[36] A. N. Pisarchik, Yu. O. Barmenkov, and A. V. Kiryanov, Phys. Rev. E **68**, 066211 (2003).
[37] R. J. Reategui, A. V. Kir'yanov, A. N. Pisarchik, Yu. O. Barmenkov, and N. N. Il'ichev, Laser Phys. **14**, 1277 (2004).
[38] A. N. Pisarchik, A. V. Kir'yanov, Yu. O. Barmenkov, and R. Jaimes-Reátegui, J. Opt. Soc. Am. B **22**, 2107 (2005).
[39] See Supplemental Material at http://link.aps.org/supplemental/10.1103/PhysRevE.86.056219 for details on the Probability densities and for differences between probability densities obtained with uniform and Gaussian noise for several regimes.
[40] F. Bonani and G. Ghione, *Noise in Semiconductor Devices*, Springer Series in Advanced Microelectronics, Vol. 7 (Springer, Berlin, 2001).
[41] S. Foster, G. A. Cranch, and A. Tikhomirov, Phys. Rev. A **79**, 053802 (2009).